JOURNAL OF MATERIALS SCIENCE 26 (1991) 824–834

Structural development during the extrusion of rapidly solidified Al–20Si–5Fe–3Cu–1Mg alloy

J. ZHOU, J. DUSZCZYK, B. M. KOREVAAR
Laboratory for Materials Science, Delft University of Technology, Rotterdamseweg 137, 2628 AL Delft, The Netherlands

An investigation concerning the changes of powder structure and microstructure during the extrusion of an important Al–Si–Fe–Cu–Mg alloy prepared from rapidly solidified powder has been carried out. The fragmentation of needle-shaped intermetallics in the alloy has been regarded as one of the main features of the process, which happens concurrently with the interparticle bonding and the shaping of the porous billets. The as-extruded microstructure is found to be mainly composed of the dynamically recovered α-Al matrix with numerous microcells, which are retained because of the inhibiting effect exerted by massive, fine second-phase particles on cell wall motion. Some recrystallized grains are also observed but their growth is effectively prevented. The refined intermetallics together with massive silicon particles and precipitates dispersed in the matrix can be expected to improve the thermal stability and high-temperature strength of the alloy to a great extent.

1. Introduction

The successful fabrication of the hypereutectic Al–Si alloys employing powder metallurgy techniques involving rapid solidification has been known for more than 10 years [1]. After being consolidated by extrusion, the alloys are characterized by very low values of thermal expansion coefficient and good wear resistance, owing to the high volume fraction of silicon particles embedded in the matrix of the alloys [2, 3]. Of this alloy system, Al–20Si–3Cu–1Mg alloy has recently been intensively investigated with respect to optimal processing [4–6]. With the addition of copper and magnesium, adequate strength, particularly at room temperature, has been found to be obtainable, thus opening up new applications to the alloy in the automobile industry. When this alloy is used as a high-performance material at elevated temperatures, as encountered in automotive engines, however, its strength is not very satisfactory. The reason for this is clear. Both copper and magnesium act as precipitation hardening elements, and their strengthening effect is diminished at above 150 °C because of the low thermal stability of the precipitates. Additionally, when the alloy is unavoidably exposed to a high temperature during processing, i.e. degassing, hot extrusion and solution treatment, coarsening of second phases and matrix microstructure can hardly be effectively prevented [7], and as a result the mechanical properties of final products are impaired. To get rid of these shortcomings, the addition of the transition element iron has been considered, in view of its high diffusivity in the liquid state and low diffusivity in the solid state (lower than that of aluminium and silicon) [8, 9]. These features ensure its high chemical homogeneity in the α-Al matrix and its thermal stability in both processing and service. Iron has an extremely low equilibrium solid solubility in the α-Al at room temperature, and under the condition of rapid solidification, its solubility can be extended up to 0.6 wt % [10], so that the precipitation of iron-containing phases can be expected to happen during the post-solidification processes including degassing and hot extrusion. The excess iron forms a dispersion of intermetallic compounds, which improves the structural stability of the alloy. In view of the above considerations, it is quite certain that the addition of 5% Fe to the base Al–Si–Cu–Mg alloy can make a substantial improvement in structural stability and high-temperature performance without sacrificing its original advantages. The alloy can then be potentially used as a more reliable material for pistons in the automobile industry.

However, a problem arises from the addition of iron. After atomization, a high volume fraction of needle-shaped intermetallic compounds with relatively large sizes is formed. It is well known that the distribution of intermetallics in the α-Al matrix can decisively influence the microstructural evolution during processing and the mechanical properties of final products. These influences are very much dependent upon their characteristics including size, interspacing and morphology. Obviously, the coarse needle shape of the intermetallics formed in the powder of the alloy is unfavourable not only to the fracture toughness, fatigue properties and workability of the material in subsequent processes [11], but also to the effectiveness of stabilizing the microstructure. Therefore, they must be reshaped and redistributed in the post-atomization

0022–2461/91 $03.00 + .12

processing so as to increase their number and to decrease their size and interspacing. Unfortunately, heat treatment cannot satisfy the above desire because the intermetallics cannot be resolved in the solid matrix. In this case, the refinement can only be accomplished by a deformation process, in which strain has to be sufficiently large so that the internal stress applied to the intermetallics can be in excess of their fracture strength and fragmentation can be achieved. In principle, extrusion at a sufficiently high reduction ratio should be capable of breaking up the intermetallics due to the involvement of heavy shearing in the deformation zone. Therefore, the secondary structural refinement can be integrated into the purposes of the extrusion operation during which the atomized powder particles are consolidated. Extrusion itself is a complicated thermomechanical process, and it has been studied as applied to the consolidation of rapidly solidified aluminium alloy powders for some years. However, no work with regard to the secondary structural refinement involved in the process has ever been reported.

The present work was aimed at understanding the microstructural development of the alloy, from the rapidly solidified loose powder through hot extrusion to the final engineering material, and thereby at providing the fundamentals for the optimum microstructural control. Of particular interest was the development of the intermetallics along with the deformation and bonding of the powder particles during extrusion and their effects on the microstructural evolution of the α-Al matrix.

2. Experimental details

The raw material in the form of powder particles was supplied by the Showa Denko K. K., Japan, produced by means of air atomization at a mean cooling rate of 10^4–10^6 K sec^{-1}. The nominal composition of the alloy was: 20% Si, 5% Fe, 3% Cu, 1% Mg (wt %) and balance aluminium. The as-received powder was first cold precompacted up to about 65% relative density, and then degassed at 300 °C to remove absorbed moisture and meanwhile to minimize its influence on the microstructure. Hot extrusion was carried out on a 2 MN press with a ϕ50 mm container and a round flat die. Extrusion temperature applied was 375 °C, reduction ratio 20 : 1 and ram speed 5 mm sec^{-1}, leading to a mean strain rate of 3.8 sec^{-1}. Before being extruded, the precompacts were heated and soaked in the container of the press for 20 min. After being cut from the discards, the extrudates were water quenched in an attempt to freeze in the hot-worked microstructure. There was some time delay in this procedure owing to the operational limitations. Additionally, some of the extrusion operations were terminated when a part of a billet was extruded, in order to investigate the course of powder particle deformation and intermetallic fragmentation during extrusion. The partially extruded billets were water quenched immediately after being ejected from the heated container.

The distribution of powder particle size was analysed using a Malvern 2600 laser particle sizer. Observations of powder particle morphology were made under a Jeol JXA 50A scanning electron microscope (SEM) operating at 15 kV, for which the powder particles were distributed evenly on a mount with a double sided tape, followed by a gold deposition procedure. Energy dispersive X-ray (EDX) analysis and X-ray mapping of powder particle cross sections were done using a Tracor microanalysis system attached to the SEM working at 20 kV, for which powder particles were embedded in a conductive resin and then polished. Optical specimens were prepared from the powder and partially extruded billets, using usual metallographic techniques. They were finally etched in a modified form of Keller and Wilcox's reagent and observed under Leitz and Neophot-2 (Carl Zeiss, Jena) microscopes for macrostructural and microstructural examinations, respectively. Transmission electron microscopy (TEM) was performed using a Philips EM400T operating at an accelerating voltage of 120 kV. EDX on the TEM was also used to aid phase identification. TEM specimens were punched out from the transverse slices of the extrudates into 3 mm discs. A variety of chemical solutions failed to polish the discs of the alloy during double jet thinning under different working conditions. Thus thinning was achieved by ion beam milling operating initially at a voltage of 6 kV and a gun inclination angle of 20°, followed by a final 0.5 h thinning at 3.5 kV and 13°.

3. Results and discussion

3.1. Characteristics of the powder particles

The as-received powder was first subjected to compositional analysis using atomic absorption spectrophotometry [12]. The results show that the alloy contains 19.2% Si, 3.24% Cu, 1.18% Mg, 5.17% Fe (wt %) and balance aluminium, which does not deviate very much from the nominal composition. The typical morphology of the powder particles as observed under SEM is given in Fig. 1. The powder particles exhibit rather rough surfaces and irregular shapes, irrespective of their sizes. Many of them are tear-drop like. This is because the oxide film that formed on the surfaces of atomized droplets during powder production prevented them from spheroidizing [13]. The size distribution of the powder particles determined by the laser sizer is presented in Fig. 2, showing that although the size varies widely between 6 and 260 μm, 90% of them are smaller than 150 μm. A considerable proportion of the powder particles fall in the size band around the mass median size of 63.7 μm. Understanding this powder particle size distribution is very important, because it predetermines all the microstructural characteristics of the material such as the scale of heterogeneity and the sizes of grains and second phases throughout the processing route.

The cross section microstructure of the powder is shown in Fig. 3, which consists of silicon particles and needle-shaped intermetallics dispersed in the α-Al matrix. The grain structure of the matrix was not discernible under the optical microscope at magnifications up to 2000. It can be seen that the silicon par-

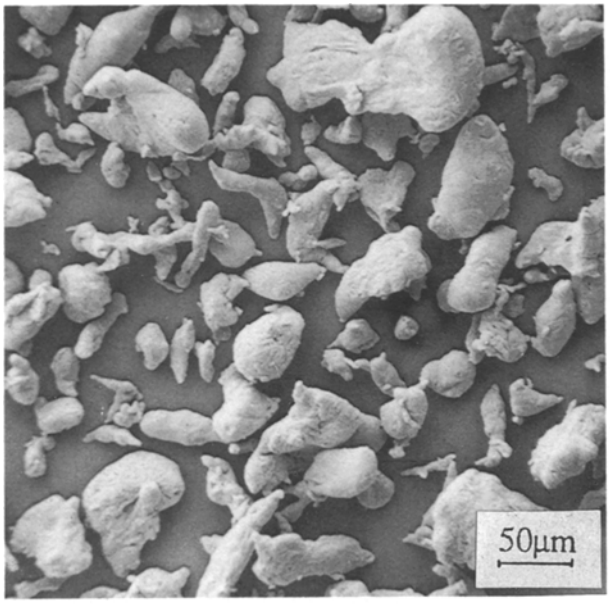

Figure 1 Typical morphology of the air atomized powder particles.

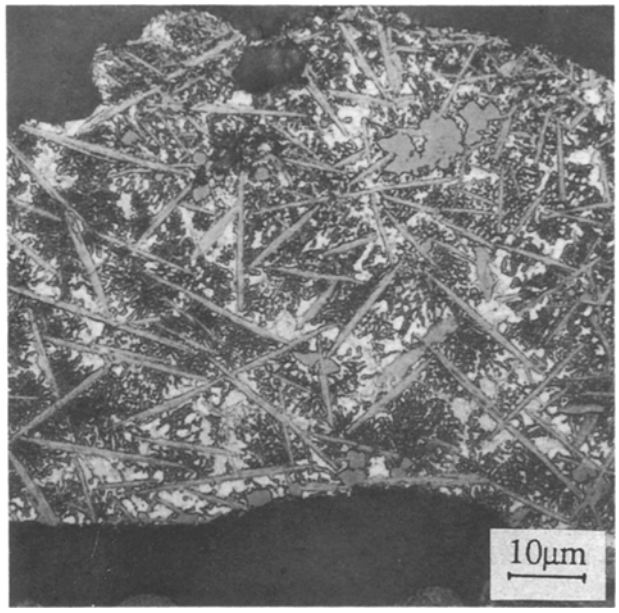

Figure 3 Optical micrograph of the powder showing the needle-shaped intermetallics and silicon particles.

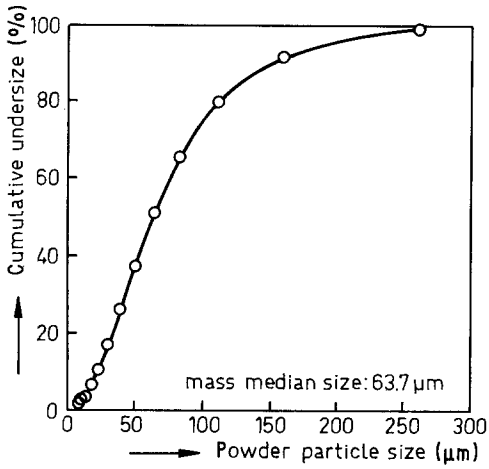

Figure 2 Size distribution of the powder particles.

ticles exhibit a bimodal distribution in size, block-like and granular. The former has an average size of about 5 μm and the latter of 0.3 μm. This phase was identified by the EDX analysis in a number of particles. It can also be observed that the needle-shaped intermetallics are randomly distributed. Their size depends strongly on individual powder particle sizes, varying between 5 and 20 μm in length. For each powder particle, the needles in the center are apparently longer than those close to the periphery (Fig. 3), indicating a relatively lower cooling rate in the particle interior during powder production which allowed the diffusional growth of the needles within the interior space available.

The SEM image of the intermetallics and X-ray mapping of Fe$K\alpha$ and Si$K\alpha$ on the cross section of a representative powder particle are presented in Fig. 4. It is clear that after atomization a small amount of iron is retained in the α-Al, but that most of the iron exists in the needle-shaped intermetallics. This implies that a certain degree of supersaturation of iron in the α-Al is attainable under the condition of air atomization. Silicon is not only concentrated in silicon particles (as shown in Fig. 4c), but also present in the acicular intermetallics. It should be noted that the Si$K\alpha$ signal scattering in the X-ray image mostly comes from the fine, granular silicon particles with reference to the optical observation (Fig. 3). Of course, a certain amount of silicon can also be supersaturated in the α-Al matrix, due to the fact that with the application of splat technique of rapid liquid quenching a high metasolubility of silicon in the α-Al up to 11 at % can be attained [14], although its maximum equilibrium solubility at the eutectic temperature of 577 °C is only 1.59 at % [15]. Mapping of Cu$K\alpha$ and Mg$K\alpha$ indicates that these elements are mostly dissolved in the matrix. Therefore, precipitation of Fe-, Si-, Cu- and Mg-containing phases on a very fine scale can be anticipated during the post-atomization processing, e.g. during degassing and extrusion.

EDX analysis reveals that the needle-shaped intermetallics contain aluminium, iron and silicon elements. Although the relative concentrations of these elements can be computed from their intensities in the spectra compared to the stored standard spectra of pure elements, the needles still cannot be assigned to a particular phase, because the intermetallics, depending upon cooling rates, can emerge in various phases with similar chemical compositions and morphologies [16]. Unfortunately, there is no information available regarding the phase constituents of this highly alloyed aluminium. As indicated in a previous study on a similar alloy using X-ray diffraction, the identification of the intermetallics is very difficult, because of the complexity in both alloy composition and solidification conditions [2]. Nevertheless, it is very likely that they are metastable and can be transformed to more thermally stable variants in the subsequent processes.

3.2. Development of powder structure during extrusion

An observation of powder particle deformation during extrusion can help understand the microstructural

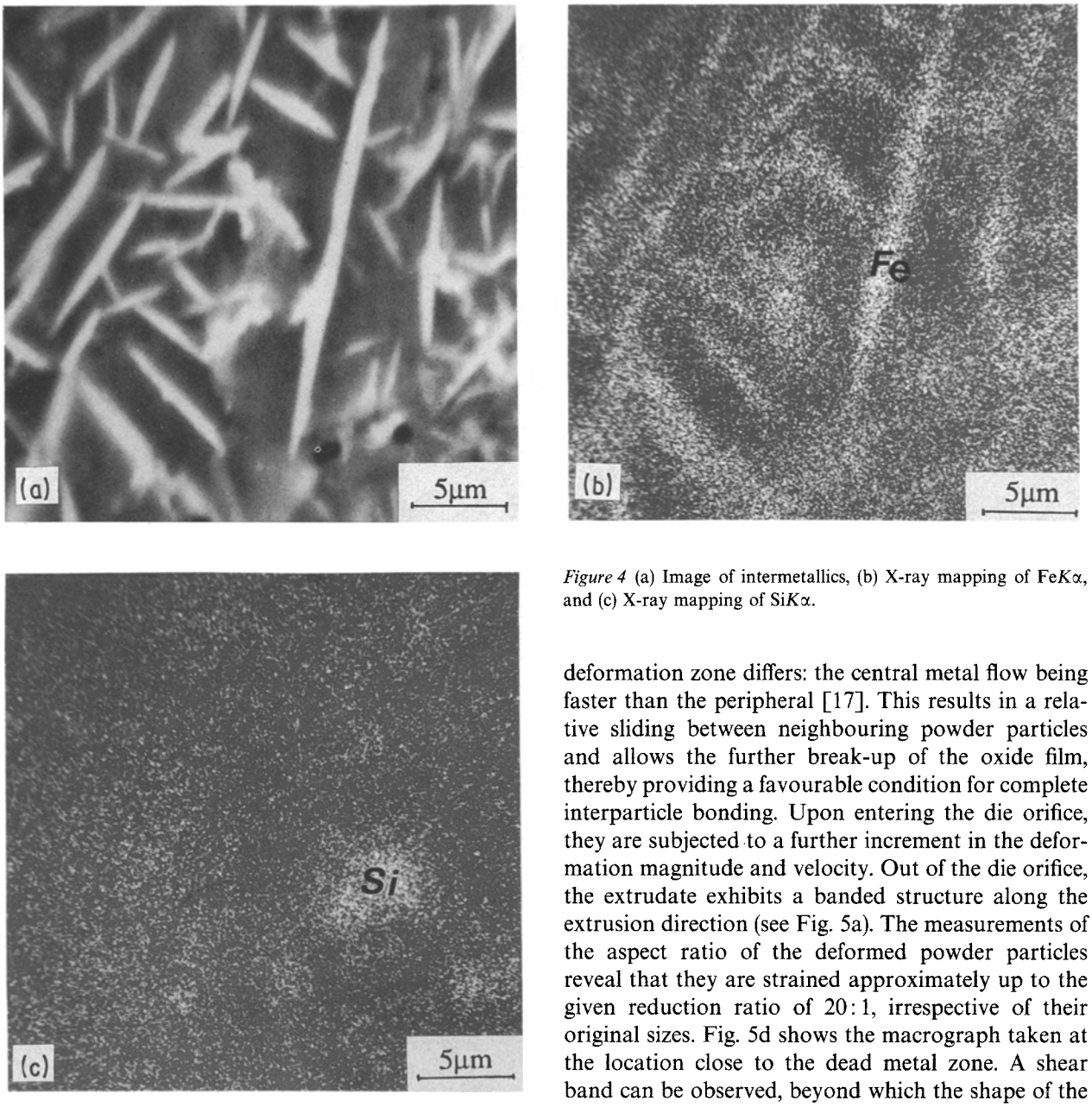

Figure 4 (a) Image of intermetallics, (b) X-ray mapping of Fe$K\alpha$, and (c) X-ray mapping of Si$K\alpha$.

development that will be discussed later. Fig. 5 shows a set of macrographs taken from five representative locations in a billet partially extruded beyond the pressure peak. It can clearly be seen that in the rear part of the billet (Fig. 5c), intimate contact between powder particles has been attained, but their shape remains almost unchanged. The original powder particles are clearly distinguishable. It suggests that the compression pressure, though high (about 780 MPa), cannot bring about large deformation of the powder particles and thus significant microstructural changes can hardly be expected. Large deformation starts only as powder particles approach the die entry (see Fig. 5b). In this zone, the powder particles, under the ram pressure, are forced to undergo a sudden, large reduction in transverse area, and thus a very high internal shear stress results. It is this stress that gives rise to the breakage of the oxide film on powder particle surfaces and microstructural modification. Furthermore, owing to the occurrence of material-tool frictions during extrusion, the longitudinal flow rate of material in the deformation zone differs: the central metal flow being faster than the peripheral [17]. This results in a relative sliding between neighbouring powder particles and allows the further break-up of the oxide film, thereby providing a favourable condition for complete interparticle bonding. Upon entering the die orifice, they are subjected to a further increment in the deformation magnitude and velocity. Out of the die orifice, the extrudate exhibits a banded structure along the extrusion direction (see Fig. 5a). The measurements of the aspect ratio of the deformed powder particles reveal that they are strained approximately up to the given reduction ratio of 20:1, irrespective of their original sizes. Fig. 5d shows the macrograph taken at the location close to the dead metal zone. A shear band can be observed, beyond which the shape of the powder particles is unaffected. The powder particles upward (Fig. 5e) are oriented along the metal flow toward the die entry, probably by the mechanisms of tilting and relative sliding. The above observations lead to the conclusion that large deformation during extrusion only happens in a very small zone restricted to the die entry.

3.3. Microstructural development during extrusion

Fig. 6 illustrates the optical microstructures as observed at the locations corresponding to those in Fig. 5 in the partially extruded billet. In the rear part of the billet, the size and distribution of the needle-shaped intermetallics (Fig. 6c) are not different from those in the loose powder. At the location (b), where the deformation zone is situated, many of the needles have been chopped up. As shown above, when the powder particles approach the die entry, they undergo a sudden increase in strain and strain rate. As a result, dislocations quickly generate and multiply. Some dislocations that cannot bypass the needles accumulate

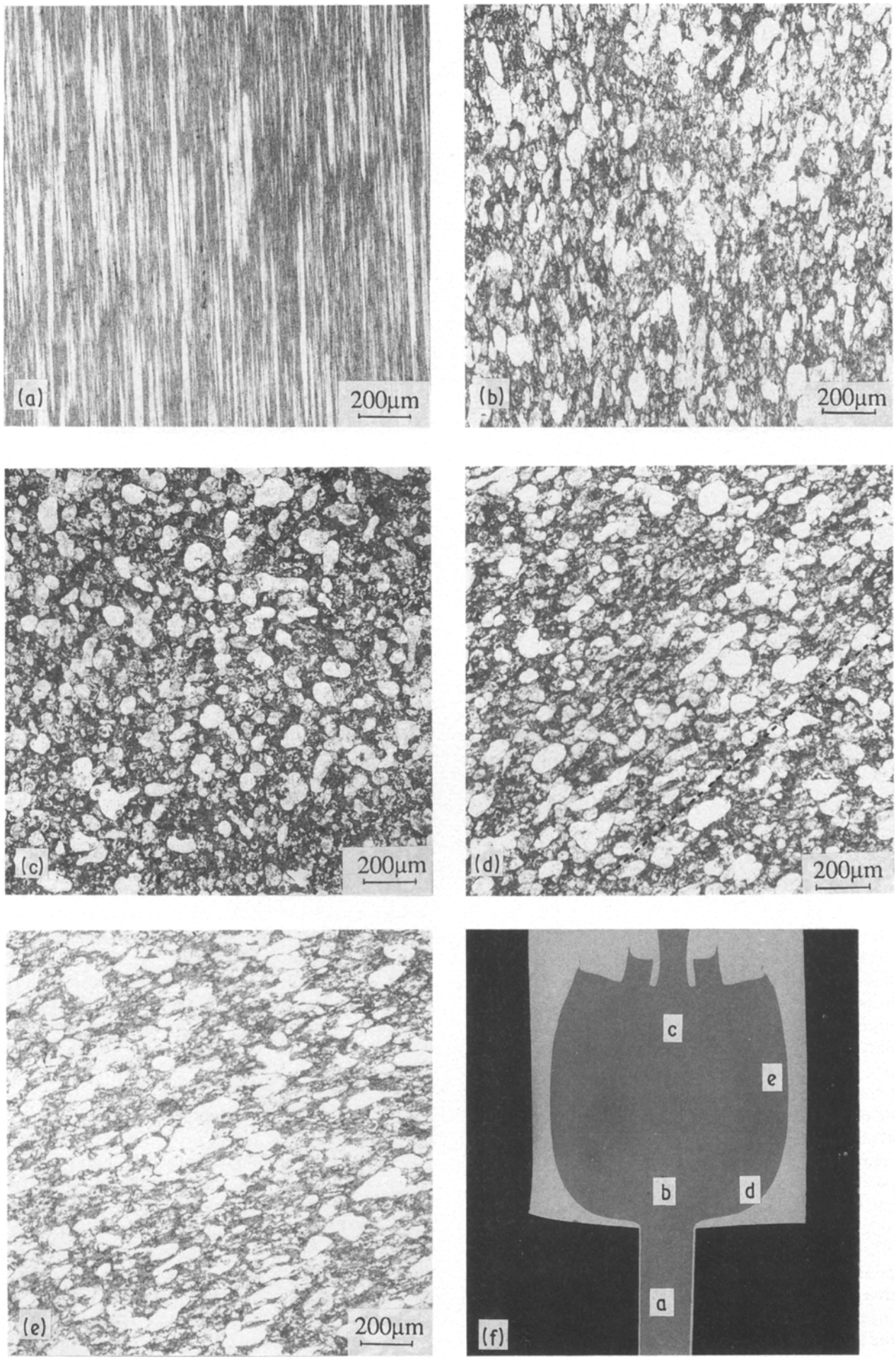

Figure 5 Macrostructures of a partially extruded billet at the different locations: (a) out of die orifice, (b) at the die entry, (c) in the rear part, (d) close to the dead metal zone, (e) close to periphery, and (f) partially extruded billet indicating the observed locations.

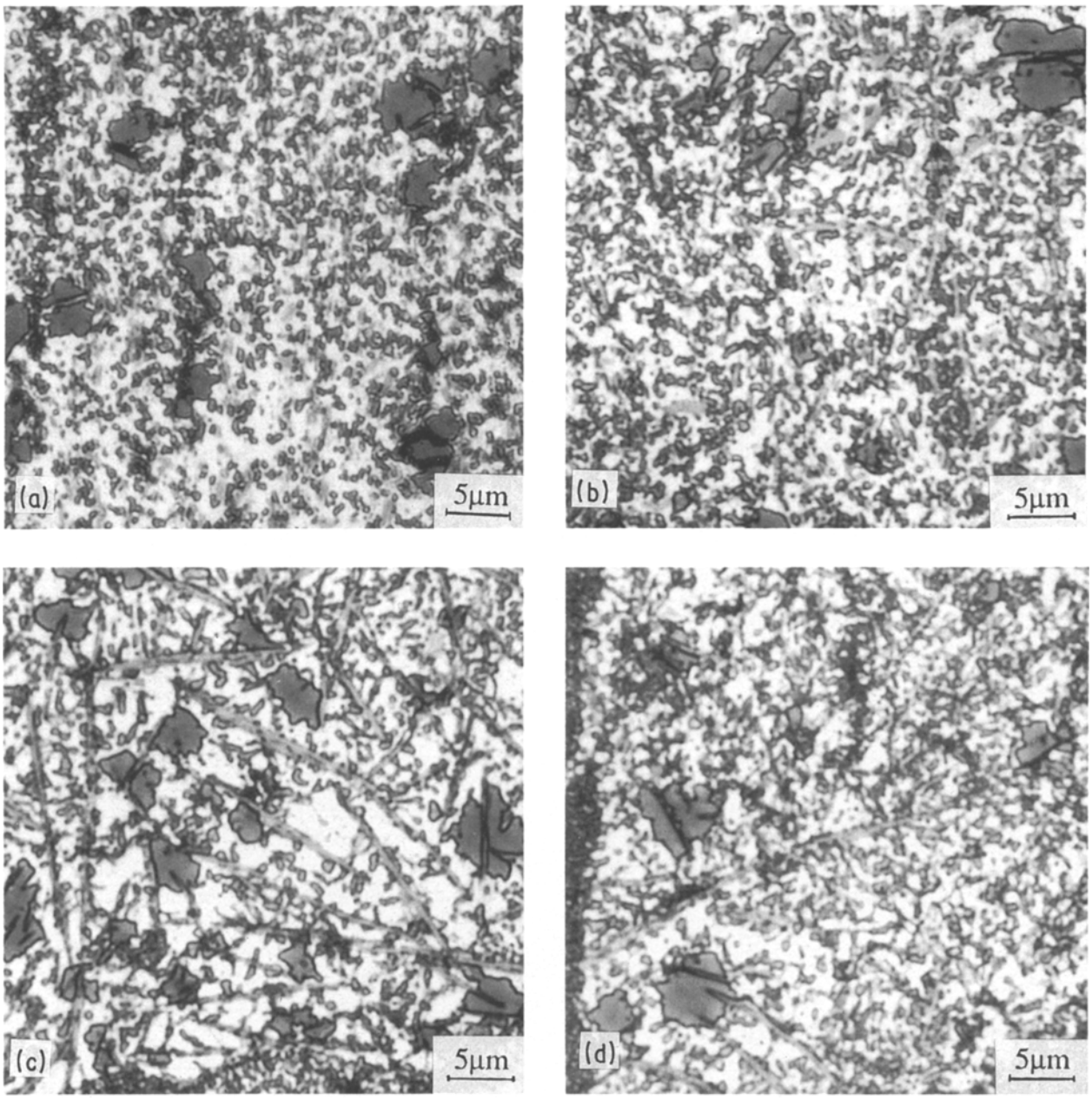

Figure 6 Microstructures of a partially extruded billet observed at the locations corresponding to Fig. 5.

along the needle length, giving rise to a localized stress concentration at the interfaces between the intermetallics and matrix. At the same time, the massive, hard silicon particles surrounding the needles with a certain spacing exert an additional bending stress on the intermetallics because of the increased stresses around them. Since the intermetallics are fairly brittle at the extrusion temperature, the bending results in the fracture of the needles. From the micrographs it can be seen that at the location (b) the fragmentation is not complete, but passing through the die orifice the intermetallics are further broken and redistributed in the spacing between silicon particles. The fragments of the intermetallics (light grey coloured) cannot be very clearly seen from the optical micrograph due to their low contrast with the matrix (see Fig. 6a). Under the optical microscope, most of the fractured intermetallics have the size of about 1 μm, but those nearby the block-like silicon particles are apparently larger.

These fragments can be expected to influence the evolution of the matrix microstructure and the resultant mechanical properties because the intermetallics with increased number and decreased interspacing will interact more effectively with dislocations and internal boundaries. At the location (d), i.e. outside the dead metal zone, a few intermetallic needles have been fractured, while upwards (Fig. 6e) their shape has not been changed at all, implying that heating to the extrusion temperature and compression with the high force cannot create any changes of the existing intermetallic morphology. Therefore, the fracture of the intermetallics during extrusion occurs only in the cone-shaped deformation zone where large powder deformation and interparticle bonding also take place.

The comparison of the microstructures before and after the extrusion (Figs 3 and 6a) indicates that some growth of silicon particles occurred during the extrusion due to the combined effect of heat and deformation. The granular silicon particles in the extrudates are about 0.5 μm in size under the optical microscope. They have been brought together by the metal flow during extrusion, leading to some silicon depleted area, particularly near the block-like silicon particles. Some longitudinal arrays of the silicon particles are observable. There is, however, no evidence of silicon particle fracture, as reported [18]. Since the silicon particles are very hard at the extrusion temperature, they do not shear, so that dislocations cannot pass through them and the deformation process of the material becomes very complicated. The influence of the silicon particles on the deformation mechanisms of the matrix operating during the extrusion will be discussed later together with the microstructural observations under the TEM.

3.4. Microstructure of the extrudate

A typical TEM microstructure of the extrudate is given in Fig. 7a, showing a mixture of the grains with and without cellular substructure and a dispersion of intermetallic particles. A principal microstructural feature of the extrudate are the grains with the substructure, which are shown in Fig. 7b and c at high magnifications. It can clearly be seen that the presence of the cellular substructure is often accompanied by the fine intermetallic particles, many of which lie at the microcell walls (Fig. 7b). The cells with clear walls (Fig. 7c) are neither uniform in size nor equiaxial in shape. Electron diffraction reveals very low misorientations between neighbouring cells, as indicated by low contrast. An appropriate estimation of the mean cell size is difficult because their size varies considerably, hence preventing the correct determination of the mean value by measuring linear intercept length. No systematic correlation between cell size and intermetallic spacing has been found. However, there is no doubt that the characteristics of the cellular substructure are associated with the distribution of the intermetallic particles in the α-Al matrix, which effectively restrict the motion of dislocations and increase dislocation density. They force dislocations to bypass them by cross-slip and climb mechanisms over a limited distance. Under these circumstances, the dislocations can only rearrange themselves by annihilating nearest redundant pairs to attain a low energy configuration and hence the cell walls are formed. After the deformation, the internal dislocations move to sinks in the cell walls, but the migration of the cell walls is prevented again by the intermetallic particles, particularly by those that are heterogeneously formed during the extrusion when the combination of high temperature and large deformation is applied. Consequently, the microcells, the direct evidence of dynamic recovery, are retained in the as-extruded microstructure. Clearly, the retention of this evidence is largely contributed by the intermetallics which stabilize the worked microstructure at the extrusion temperature by inhibiting the motion of cell walls. Therefore, dynamic recovery through the formation of microcells can be concluded to be the principal restoration mechanism of the alloy in extrusion.

The grains without the cellular substructure are mostly equiaxial. Being free of any internal dislocation tangles, they are most likely formed statically during the time interval between the ceasing of extrusion and quenching. It has been found that, for commercially pure aluminium, the occurrence of partial static recrystallization is just a matter of a fraction of one second after hot compression under certain conditions [19]. In the extrusion of copper the nucleation of recrystallization has been suggested to happen concurrently with dynamic recovery [20]. Of course, the recrystallization nucleation can be promoted or prevented depending on the stacking fault energy of material and the characteristics of second-phase particles. For the present alloy, the latter factor should be more pronounced, because in the extrudates of the base Al–20Si–3Cu–1Mg alloy the recrystallized grains are much less observed [6]. The observations on the present alloy imply that although the stored strain energy in the material is considerably reduced by forming arrays of cell walls during extrusion, the residual energy is still at a high level, so that the material has a strong tendency to static or metadynamic recrystallization. Clearly, the very fine intermetallic particles in the alloy inhibit the completion of dynamic recovery. Their retarding effect on recrystallization can be reduced after the large deformation during extrusion [21]. Hence, recrystallization may intervene at some favourable sites, immediately after deformation, possibly even without the need of an incubation period. At least, the present as-extruded microstructure confirms that under certain conditions recrystallization nuclei can be formed concurrently with or before the polygonization of substructure [22].

Fig. 7d shows the outcrop of a recrystallized grain which is obstructed by the intermetallics. The obstruction to the growth of the new grain results in a complex stress state in the surrounding matrix, as clearly indicated by a high density of dislocation arrays. It can also be noticed that the second-phase particles are often absent from the interior of newly formed grains, but stationed at the periphery. The preferred sites of recrystallization nucleation are usually at the conjunctions of original grain boundaries or in the vicinity of

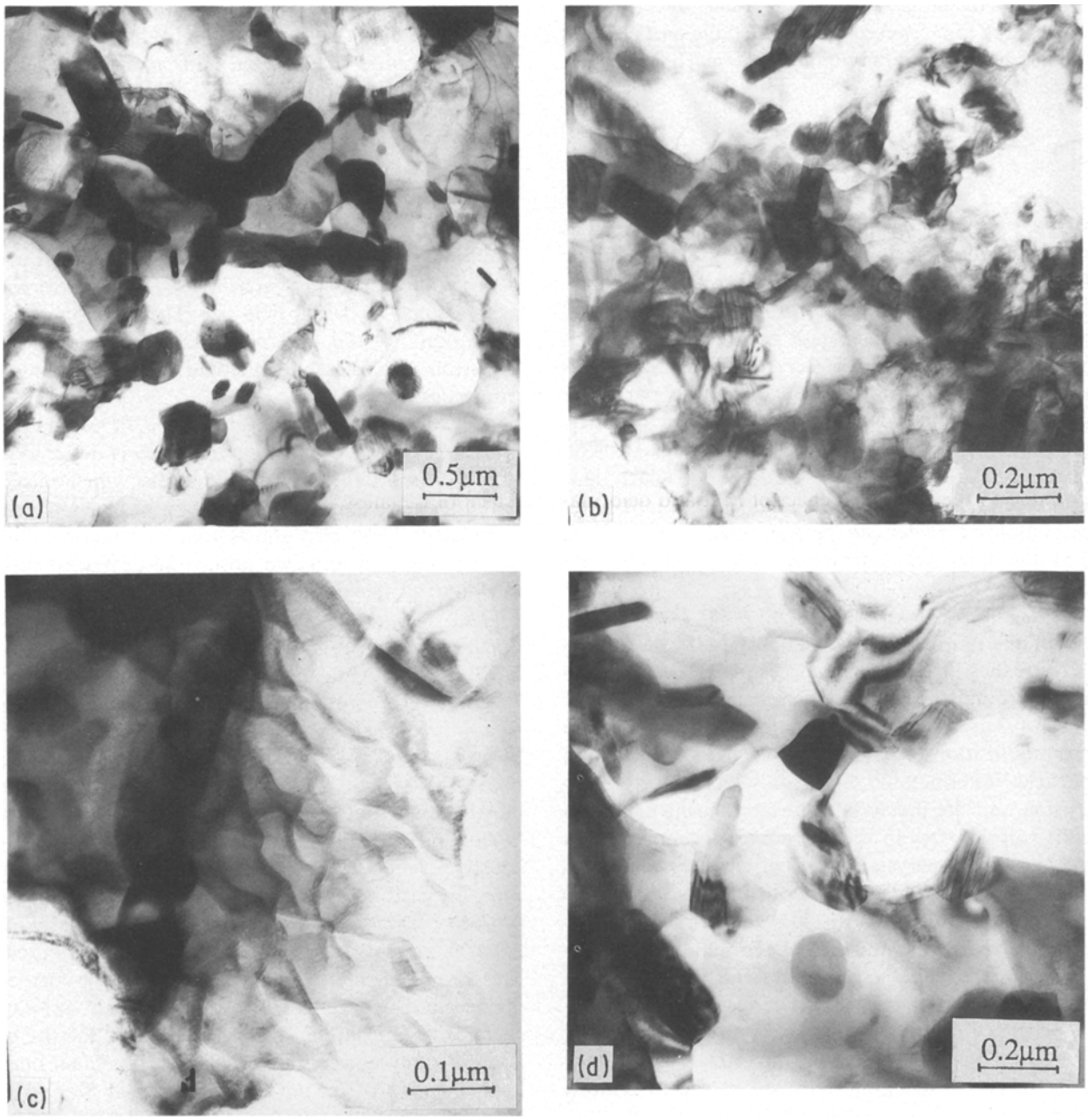

Figure 7 As-extruded microstructure of the alloy: (a) general microstructure showing the mixture of recovered and recrystallized grains, (b) grains with the microcells associated with intermetallics, (c) cells with clear walls, (d) outcrop of a recrystallized grain surrounded by intermetallics with a certain spacing, (e) growth of a recrystallized grain into deformed grains.

large second-phase particles [23]. The new grain in the interior of a deformed grain, as observed in Fig. 7d, may be originated from a favourable site below the observation surface [24]. Fig. 7e shows the growth of a newly formed grain into the deformed ones with a high density of cell walls. Clearly, the growth is difficult owing to the presence of the needle-like intermetallic particle. There is much evidence under the TEM that the refined intermetallics in the alloy act as effective obstacles to the migration of newly formed grain boundaries and the growth is generally confined within the spacing of the particles. It is quite possible to establish an equilibrium quickly during the time delay before the quenching operation, between the driving force for complete recrystallization and the

resistance to the growth of new grains, including the Zener drag force caused by intermetallic particles and the increment in grain boundary energy [25], which is given by:

$$F_R = F_G + F_Z \quad (1)$$

or

$$R_C = 2\gamma/(F_R - 3f/2r) \quad (2)$$

where F_R is driving force for recrystallization, F_G is grain-boundary shrinkage force, F_Z is Zener pinning force, R_C is critical grain size for growth, γ is grain boundary energy, and f and r are volume fraction and mean radius of second-phase particles, respectively. Therefore, the kinetics of recrystallization growth is mainly governed by the f/r value for a particular material under a given working condition. Obviously, the refinement of intermetallics during the extrusion increases the critical grain size, above which new grains can grow. It means that an increased number of recrystallized nuclei can be prevented from growth, and the final grain structure will be significantly refined.

It has been known that second-phase particles larger than 1 μm basically act as recrystallization nuclei because they bring about complex plastic deformation zones around them, while the second-phase particles of 0.1–0.2 μm usually exert a major inhibiting effect on recrystallization [26]. The coexistence of the silicon particles, intermetallic dispersoids formed before extrusion and the precipitates formed during extrusion with various sizes in the extrudates certainly makes the kinetics of recrystallization of the alloy very complicated. It is possible that the silicon particles and the intermetallics that are not completely broken into fine rods are active in stimulating the formation of recrystallization nuclei in their vicinities. It is very clear from the observations that the massive, very fine intermetallic particles largely prevent the recrystallization by pinning cell walls, and inhibit the growth of the statically recrystallized grains formed at the favourable sites by Zener drag mechanism. In view of these considerations, the bimodal distribution of the second-phase particles in the present alloy is beneficial for maintaining very fine grain size in the subsequent forming and heat treatment, when the alloy is expected to be completely recrystallized. This is similar to the technique known as discontinuous recrystallization, one of the effective ways to refine microstructure in wrought aluminium alloys with bimodal distribution of second-phase particles [27]. According to the Zener drag model [28], the critical grain radius for stability, R_{crit}, is given by:

$$R_{crit} = 4r/3f \quad (3)$$

in which r and f have the same meaning as before. The equation indicates that the grain size obtained after complete recrystallization is controlled by the r/f value. The refinement of intermetallics during extrusion decreases the r/f value, and thus restricts the growth of matrix grains due to increased pinning. Therefore, it benefits the thermal stability of the grain structure in the final products and the combination of strength and ductility of the alloy.

Because of the coexistence of the deformed and recrystallized grains in the as-extruded microstructure, there is no practical meaning to measure grain size for the application of Hall–Petch relationship. In this case, it is suggested to relate the microstructure and strength by using the following correlation [29]:

$$\sigma \propto fd^{-1}(1 - f)^{-1} \quad (4)$$

where d and f are the mean diameter and volume fraction of second-phase particles, respectively. It can be seen that at a given f-value, the strength is inversely proportional to the particle size. Therefore, the fragmentation of the intermetallics achieved during extrusion will directly contribute to the mechanical properties of the alloy.

According to the results from the EDX analysis attached to the TEM, only aluminium is detected in the deformed and newly formed grains, which means that after extrusion the precipitation has been almost completed. TEM also shows that the intermetallics can be classified into two groups according to their morphology, the needle-like and globular, as shown in Fig. 8a. The needles have lengths between 0.5–1 μm under the TEM, randomly distributed in the matrix. EDX analysis indicates that they are Al-, Si- and Fe-containing compounds. X-ray diffraction suggests that most of them can be denoted as the equilibrium phase β(Al, Fe, Si), transformed from the metastable phase δ(Al, Fe, Si) [2]. The globular particles are mostly situated at the cell walls, grain boundaries or Y junctions (Fig. 8b), implying they were heterogeneously precipitated during the extrusion processes. They are distributed non-uniformly, and aggregation can be observed. Because of this, electron diffraction patterns are rather difficult to be uniquely indexed. This group of intermetallic particles can be further divided into two kinds which differ in their size and chemical composition. The large ones have the size of about 0.2 μm and contain Al–Si–Fe. The small ones have the size of 0.1 μm and contain Al–Si–Fe–Cu elements. The latter kind of the particles, shown in Fig. 8c, most effectively stabilize the recovered microstructure. Previous work has shown that it is not an unusual problem to identify phases in complex aluminium alloys, particularly undergone rapid solidification, by using techniques like X-ray diffraction or electron diffraction [30–32]. Nevertheless, there is still a need of further work on the identification of the unknown phases present in the complicated alloy under study.

Fig. 9 shows a granular silicon particle with the size of about 0.5 μm in the as-extruded α-Al matrix, which was identified with selected area electron diffraction. During extrusion, the presence of the silicon particles undoubtedly creates extra deformation zones in their vicinities, because of their non-deformability. For the particles with this size, local lattice rotations should be an important mechanism to accommodate the heterogeneous plastic deformation for maintaining the continuity between the particles and matrix [33]. But high dislocation density or misorientation in the surroundings of the silicon particles is not found, as indicated by low contrast (see Fig. 9). This observation is not

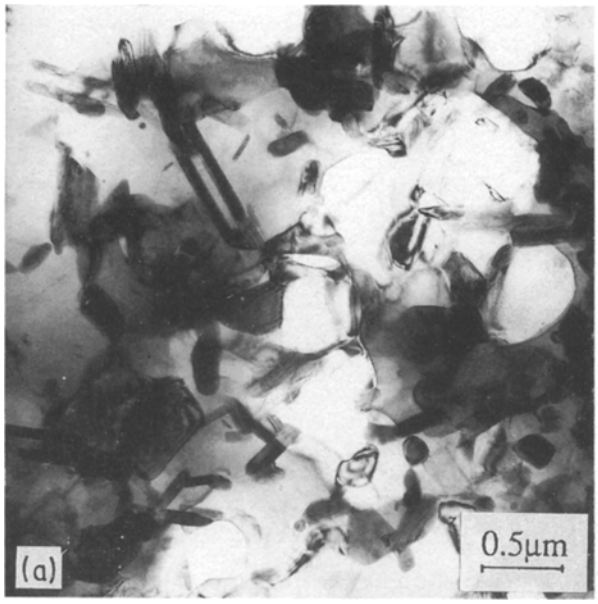

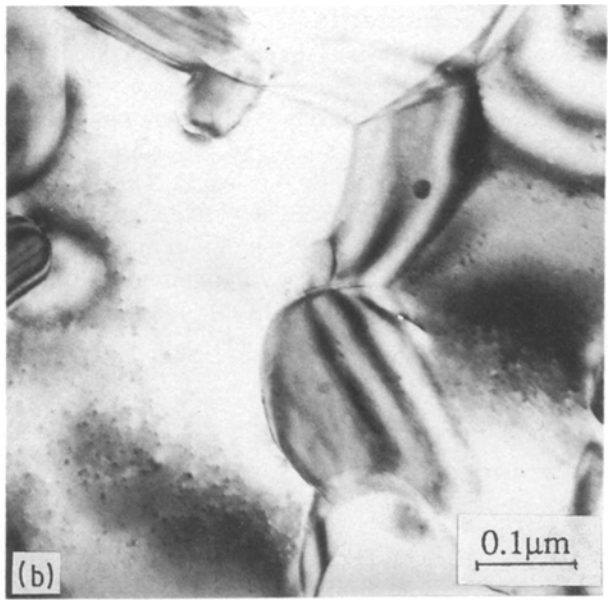

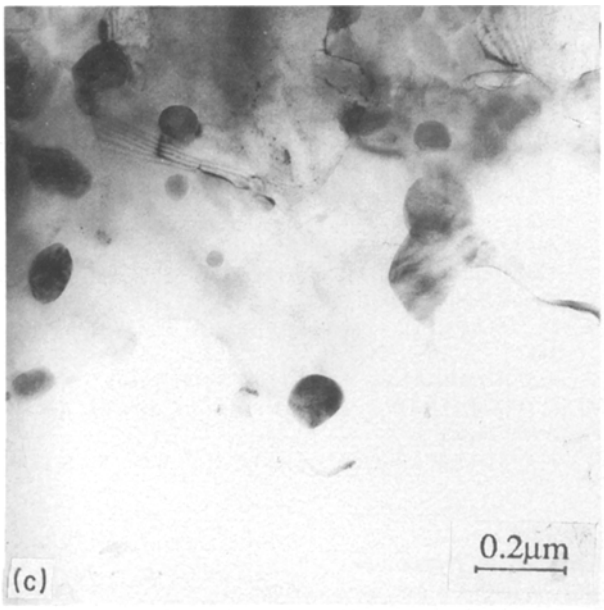

Figure 8 (a) Distribution and morphologies of intermetallic particles in the extrudates, (b) particles at grain boundaries and Y junctions, and (c) very fine precipitates in the deformed grains.

consistent with that in Al–Si dual-phase alloys [34]. The reason might be that the fine intermetallics with the size of about 0.2 μm in the vicinities suppressed the occurrence of rotations and even the formation of microcells [35]. But we think it more likely that recrystallization around the silicon particles occurred during the time delay before quenching, which reduced the misorientation and eliminated the substructure.

4. Conclusions

1. The large deformation and bonding of the powder particles during extrusion only happen in the cone-shaped deformation zone; and at the same time the needle-shaped intermetallic compounds formed during powder production are fragmented resulting from the plastic flow of the matrix.

2. The as-extruded microstructure of the alloy is composed of fine grains with and without cellular substructure. During extrusion the motion of dislocations is restricted and afterwards cell walls are pinned by the intermetallics with a high volume fraction. The evidence of dynamic recovery is thus retained.

3. Initial recrystallization occurs quickly after deformation at some favourable sites, but the growth of the newly formed grains is effectively prevented by the fine second-phase particles by the Zener drag mechanism.

4. The fragmented intermetallics, the fine precipitates formed during extrusion and silicon particles form a bimodal distribution of second-phase particles, which substantially increases the thermal stability of the matrix structure by inhibiting the growth of grains, and contributes to the combination of strength and ductility of the alloy.

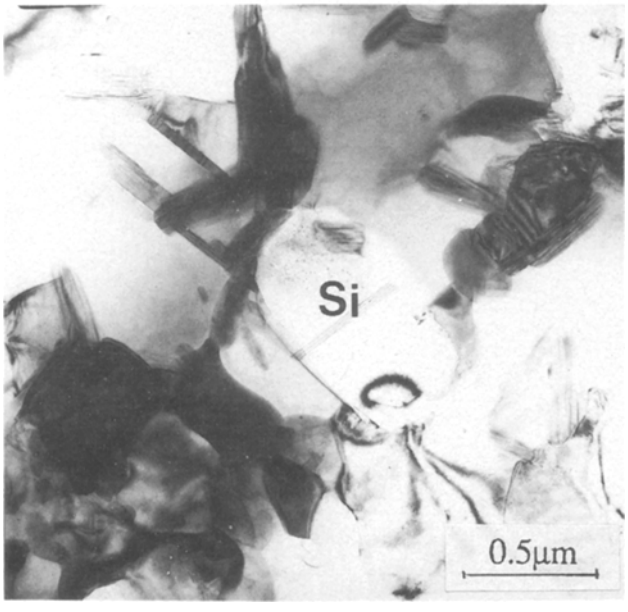

Figure 9 A silicon particle in the matrix with intermetallic particles.

Acknowledgements

The authors would like to thank Ing. E. J. A. van Dam and Mr C. D. de Haan for their assistance with SEM and TEM work, respectively. Thanks are also due to the Showa Denko K. K., Japan, for supplying the atomized powder used in this work. The financial support of the Royal Academy of Science in The Netherlands (KNAW), the Foundation for Technological Research (STW) and the Foundation for Fundamental Research of Matter (FOM) is gratefully acknowledged.

References

1. H. M. SKELLY and C. F. DIXON, *Int. J. Metals Powder Metal.*, **3** (1971) 47.
2. T. HIRANO and T. FUJITA, *Trans. Jpn Institute Light Met.* **37** (1987) 670.
3. T. FUJITA, F. KIYOTA, T. HIRANO and Y. KOJIMAT, *ibid.* **37** (1987) 677.
4. N. KUROISHI, Y. ODANI and Y. TAKEDA, *Met. Powder Report* **40** (1985) 642.
5. J. ZHOU and J. DUSZCZYK, *J. Mater. Shaping Technol.* **6** (1989) 241.
6. J. ZHOU and J. DUSZCZYK, in Proceedings of the 1st European Conference on Advanced Materials and Processes, Aachen, West Germany, November 1989, in press.
7. J. ZHOU and J. DUSZCZYK, *J. Mater. Sci.*, **25** (1990).
8. R. YEARIM and D. SHECHTMAN, *Metall. Trans. A* **13A** (1982) 1891.
9. G. THURSFIELD and M. J. STOWELL, *J. Mater. Sci.* **9** (1974) 1644.
10. H. JONES, *Mater. Sci. Eng.* **5** (1969/70) 1.
11. Y. TAKEDA, T. HAYASHI, Y. ODANI, N. AMANO and N. KUROISHI, "Hot Forgeability of Hot Extruded PIM Al–Si–Fe–X Alloys", Private Communication, Sumitomo Electric Industries Ltd., Japan.
12. J. L. ESTRADA and J. DUSZCZYK, *J. Mater. Sci.*, **25** (1990) 886.
13. K. AKECHI, Y. ODANI and N. KUROISHI, *Sumitomo Electric Technical Review* **24** (1985) 191.
14. M. ITAGAKI, B. C. GIESSEN and N. J. GRANT, *Trans. ASM* **61** (1968) 330.
15. M. HANSEN, "Constitution of Binary Alloys" (McGraw-Hill, New York, 1958).
16. P. LIU and G. L. DUNLOP, in "Aluminium Alloys—Their Physical and Mechanical Properties", edited by E. A. Starke, Jr and T. H. Sanders, Jr (EMAS, West Midlands, UK, 1986) p. 3.
17. A. J. BRYANT, *Met. Technol.* **2** (1975) 21.
18. T. HIRANO, F. OHMI, S. HORIE, F. KIYOTO and T. FUJITA, in Proceedings of International Conference on Rapidly Solidified Materials, San Diego, California, Feb. 1986, edited by P. W. Lee and R. S. Carbonara (ASM, Ohio, 1986) p. 327.
19. R. W. EVANS and G. R. DUNSTAN, *J. Inst. Met.* **99** (1971) 4.
20. W. PACHLA, L. STYCZYNSKI, S. POROWSKI and S. WOJCIECHOWSKI, *Met. Sci.* **16** (1982) 519.
21. N. HANSEN and B. BAY, *J. Mater. Sci.* **7** (1972) 1351.
22. R. KASPAR and J. PLUHAR, *Met. Sci.* **9** (1975) 104.
23. F. J. HUMPHREYS, *Acta Metall.* **25** (1977) 1323.
24. M. SCHWEIZER and W. FORM, *J. Inst. Met.* **101** (1973) 24.
25. H. M. CHAN and F. J. HUMPHREYS, *Acta Metall.* **32** (1984) 235.
26. F. R. CASTRO-FERNANDEZ and C. M. SELLARS, *Mater. Sci. Technol.* **4** (1988) 621.
27. D. J. LIOYD, in Proceedings of the 8th Light Metal Congress, Leoben, Austria, 1987, edited by F. Jelitsch (Aluminium-Verlag, Dusseldorf, 1988) p. 553.
28. E. NES, N. PRUM and O. HUNDERI, *Acta Metall.* **33** (1985) 11.
29. B. I. EDELSON and W. M. BALDWIN, Jr, *Trans. ASM* **55** (1962) 230.
30. H. JONES, *Aluminium* **54** (1978) 274.
31. W. M. GRIFFITH, R. E. SANDERS, Jr and G. J. HILDEMAN, in Proceedings of a Symposium on High-Strength Powder Metallurgy Aluminium Alloys, Dallas, Texas, February 1982, edited by M. J. Kozak and G. J. Hildeman (AIME, Pennsylvania 1982) p. 209.
32. G. J. MARSHALL and T. SHEPPARD, *Met. Sci.* **18** (1984) 561.
33. F. J. HUMPHREYS, *Acta Metall.* **27** (1979) 1801.
34. S. DERMARKAR, P. GUYOT and J. PELISSIER, *ibid.* **31** (1983) 1315.
35. T. C. ROLLASON and J. W. MARTIN, *J. Mater. Sci.* **5** (1970) 127.

Received 15 November
and accepted 1 December 1989